



# CT and MRI for Repaired Complex Adult Congenital Heart Diseases

Suvipaporn Siripornpitak, MD<sup>1</sup>, Hyun Woo Goo, MD, PhD<sup>2</sup>

<sup>1</sup>Department of Diagnostic and Therapeutic Radiology, Faculty of Medicine, Ramathibodi Hospital, Mahidol University, Bangkok, Thailand;

<sup>2</sup>Department of Radiology and Research Institute of Radiology, Asan Medical Center, University of Ulsan College of Medicine, Seoul, Korea

An increasing number of adult congenital heart disease (ACHD) patients continue to require life-long diagnostic imaging surveillance using cardiac CT and MRI. These patients typically exhibit a large spectrum of unique anatomical and functional changes resulting from either single- or multi-stage palliation and surgical correction. Radiologists involved in the diagnostic task of monitoring treatment effects and detecting potential complications should be familiar with common cardiac CT and MRI findings observed in patients with repaired complex ACHD. This review article highlights the contemporary role of CT and MRI in three commonly encountered repaired ACHD: repaired tetralogy of Fallot, transposition of the great arteries after arterial switch operation, and functional single ventricle after Fontan operation.

**Keywords:** *Computed tomography; Functional single ventricle; Magnetic resonance imaging; Repaired tetralogy of fallot; Transposition of the great arteries*

## INTRODUCTION

Advances in the diagnosis and treatment of pediatric congenital heart disease have resulted in improved survival rates, with many repaired patients reaching adulthood. In cases of adult congenital heart disease (ACHD), patients typically undergo palliative and/or corrective treatment with either a surgical, interventional, or hybrid procedure. The resultant changes in the cardiovascular anatomy and physiology are subject to long-term imaging follow-up to ensure adaptive responses and identify potential complications early on. The recommended frequency and modality for imaging follow-up is based on the underlying disease, mode of correction, and functional status as well as strengths and weaknesses of each modality (1).

Multimodality approaches are the standard of care for monitoring ACHD. Transthoracic echocardiography is a primary and essential tool for both anatomical and functional assessment (2). Cardiac CT and MRI have been generally regarded as complementary tools to transthoracic echocardiography (1); however, their role in evaluating ACHD is increasing because of technical advances, especially in functional and quantitative assessment (3-5). In this review, the authors describe contemporary CT and MRI evaluation of ACHD, with a focus on the three commonly encountered complex and repaired diseases: tetralogy of Fallot (TOF), transposition of the great arteries (TGA), and functional single ventricle.

## Repaired TOF

TOF is the most common type of cyanotic congenital heart disease consisting of an overriding aorta, ventricular septal defect, right ventricular hypertrophy, and right ventricular outflow tract (RVOT) obstruction. The three main surgical approaches for relieving RVOT obstruction are largely based on the severity of obstruction, integrity of the pulmonary valve, and presence of an anomalous coronary artery crossing over the RVOT: 1) annulus-sparing repair for patients with a pulmonary valve Z-score greater

**Received:** July 12, 2020 **Revised:** August 21, 2020

**Accepted:** September 1, 2020

**Corresponding author:** Hyun Woo Goo, MD, PhD, Department of Radiology and Research Institute of Radiology, Asan Medical Center, University of Ulsan College of Medicine, 88 Olympic-ro 43-gil, Songpa-gu, Seoul 05505, Korea.

• E-mail: ghw68@hanmail.net

This is an Open Access article distributed under the terms of the Creative Commons Attribution Non-Commercial License (<https://creativecommons.org/licenses/by-nc/4.0>) which permits unrestricted non-commercial use, distribution, and reproduction in any medium, provided the original work is properly cited.

than -4, 2) transannular patch repair for patients with a severely hypoplastic pulmonary valve (Z-score < -4) or atretic pulmonary valve, and 3) right ventricle-to-pulmonary artery conduit repair (Rastelli procedure) for patients with an anomalous coronary artery crossing over the RVOT (5, 6). Transannular patch repair frequently leads to RVOT dilatation and aneurysm, chronic and severe pulmonary regurgitation, and subsequent right ventricular dilatation and dysfunction (Fig. 1) (7-9). In the Rastelli procedure, conduit stenosis may occur, which often requires interventional treatment or reoperation with conduit change. Other common complications include aortic root dilatation with an incidence of 29% in adults with repaired TOF (10) and left ventricular dysfunction with an incidence of 23.6% (11). Rarely, focal (approximately 11%) or diffuse myocardial scar may occur (Fig. 1) (12).

Since repaired TOF patients with the aforementioned complications are often asymptomatic, CT and MRI, as additional noninvasive imaging methods, are frequently used not only for early detection of these complications, but also to determine the optimal timing of pulmonary

valve replacement to avoid irreversible right ventricular dysfunction (13, 14). According to the 2018 American College of Cardiology and American Heart Association guidelines for ACHD, MRI is regarded as the reference standard for evaluating right ventricular volume and function, quantification of pulmonary regurgitation, and detection of myocardial scarring (1). Traditionally, cardiac CT has rarely been considered appropriate for ACHD in situations where cardiac MRI is contraindicated or non-diagnostic (15). However, cardiac CT acquired with optimized imaging protocols is increasingly being used in patients with repaired TOF (14, 16-18).

### Morphologic Evaluation of the RVOT and Pulmonary Artery

Prior to corrective surgery, most TOF patients undergo one or more palliative procedures to promote pulmonary artery growth by placing a vascular stent. Moreover, a vascular coil may be inserted to occlude major aortopulmonary collateral, which protects the development of pulmonary vascular disease due to longstanding exposure of pulmonary vessels to systemic pressure. Due to its high spatial resolution and excellent overall image quality, cardiac CT is useful for the morphologic evaluation of the RVOT and pulmonary artery, particularly in evaluating vascular stents and prosthetic valves (17, 18). In contrast, metallic artifacts from stents (Fig. 2), coils (Fig. 3), and sternal wires considerably degrade the diagnostic performance of cardiac MRI. CT can be used to identify patients with high to intermediate risk of coronary compression by a percutaneously implanted pulmonary valve, a non-surgical procedure to reduce pulmonary regurgitation (17, 19). CT is advantageous over MRI in delineating calcified homografts prior to percutaneous pulmonary valve implantation (Fig. 4) and in monitoring the integrity and position of the implanted valve (Fig. 5). In addition to the proximal segments, the peripheral small pulmonary arteries are better delineated on CT because of higher spatial and contrast resolution than that of MRI. Therefore, CT pulmonary vascular volume ratio can be used not only to quantitate the asymmetry of pulmonary artery flow but also to evaluate the effectiveness of pulmonary artery angioplasty in patients with peripheral pulmonary artery stenosis (20, 21).

MRI can be used to evaluate the anatomical and functional diversity of the RVOT and central pulmonary arteries in patients with repaired TOF, which is a major determinant of device suitability in percutaneous pulmonary

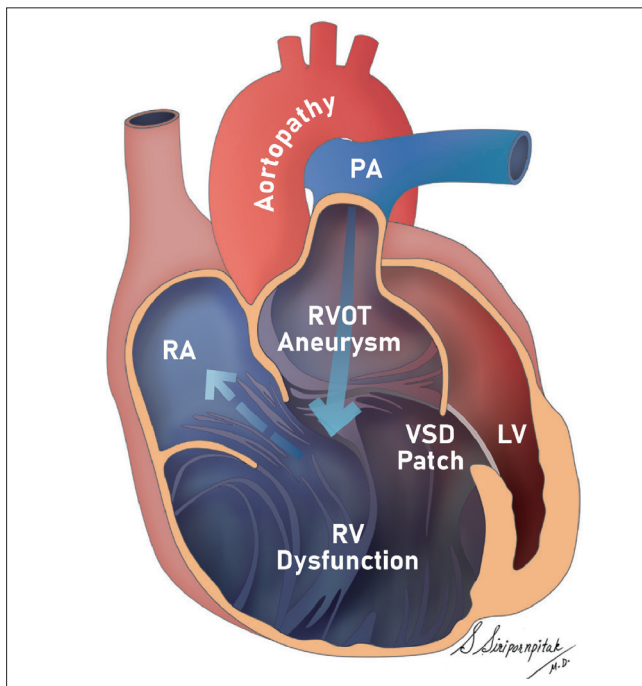


**Fig. 1. Schematic drawing illustrating sequelae after transannular patch repair in a patient with tetralogy of Fallot.** RVOT aneurysm and PR (blue solid arrow) are commonly encountered. Chronic and severe PR gradually dilates the RV, which may cause leftward bowing of the interventricular septum and squash the LV. Tricuspid regurgitation (blue dotted line) may ensue secondary to RV dilatation. LV = left ventricle, PA = pulmonary artery, PR = pulmonary regurgitation, RA = right atrium, RV = right ventricle, RVOT = right ventricular outflow tract, VSD = ventricular septal defect

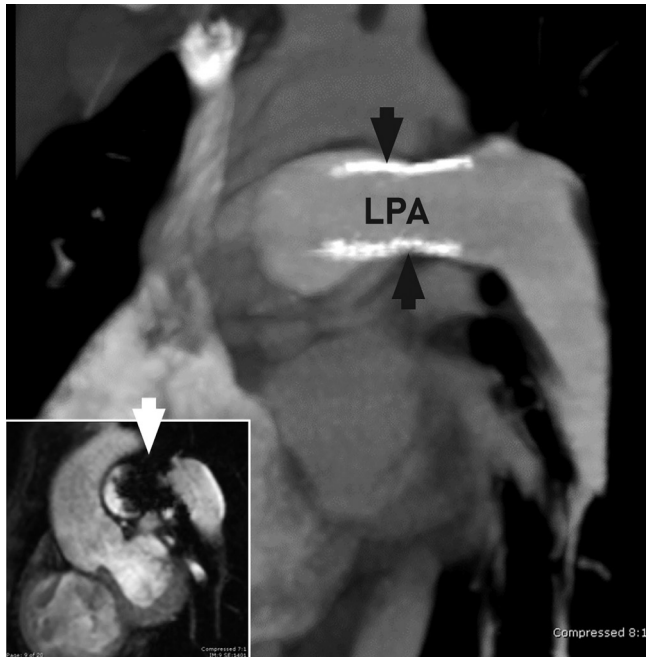


**Fig. 2.** A 12-year-old male with repaired tetralogy of Fallot. Cardiac CT image clearly demonstrates the patency of an LPA stent (black arrows). In contrast, the stent produces a metallic artifact (white arrow) obscuring the adjacent LPA on oblique sagittal cardiac MRI (small figure inserted in the left lower corner). LPA = left pulmonary artery

valve implantation (22, 23). Of the heterogeneous RVOT morphology, a pyramidal morphology related to transannular patch repair poses a risk for device dislodgement because of substantial discrepancy in size between the RVOT and the pulmonary trunk (23).

### Pulmonary Regurgitation

The pulmonary regurgitant fraction, an important hemodynamic complication in repaired TOF, may be calculated by comparing left and right ventricular stroke volumes measured using CT (24). However, this value may be misleading when regurgitation is substantial in valves other than the pulmonary valve. Therefore, it should be correctly expressed as volume load on the right ventricle rather than the pulmonary regurgitant fraction (14).

MRI using a phase-contrast pulse sequence is regarded as a standard for quantifying pulmonary regurgitation (25). The pulmonary regurgitant fraction is calculated as the retrograde flow volume divided by the antegrade flow volume (Fig. 6) (8). Notably, pulmonary flow measured using phase-contrast imaging is subject to underestimation in cases of turbulent and non-laminar pulmonary regurgitant flow, which is common in patients with repaired TOF. We may confirm the inherent underestimation of pulmonary regurgitation

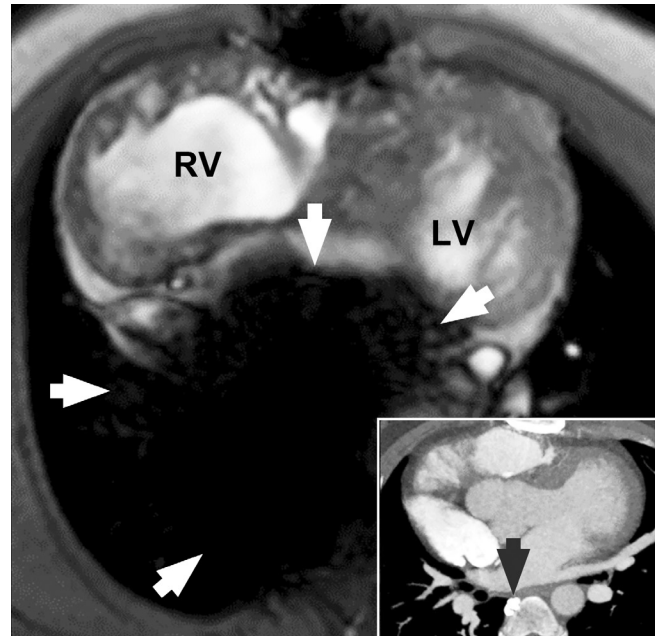


**Fig. 3.** Axial cine MRI reveals a severe artifact (white arrows) obscuring both atria in a 24-year-old male with repaired tetralogy of Fallot. The artifact is caused by a vascular coil used to occlude a major aortopulmonary collateral artery (black arrow) that is clearly seen on cardiac CT (small figure inserted in the right lower corner).



**Fig. 4.** A 24-year-old male with tetralogy of Fallot who underwent Rastelli operation. Cardiac CT performed prior to percutaneous pulmonary valve implantation reveals a focus of calcified conduit (black arrow) that is barely seen on cardiac MRI (small figure inserted in the right lower corner). In addition, the spatial relationship between the conduit and the sternum cannot be accurately evaluated on cardiac MRI due to metallic artifact (star) caused by sternal wires.

measured using phase-contrast imaging by checking the stroke volume difference between the right and left ventricles in cases with no or trivial tricuspid regurgitation.

Mild residual RVOT obstruction seems to protect against the detrimental long-term effects of pulmonary regurgitation (26). In contrast, residual or recurrent branch pulmonary artery stenosis evaluated on CT or MRI increases net pulmonary regurgitation (Fig. 7) (18, 25).

### Right Ventricular Volume and Function

Chronic and severe pulmonary regurgitation commonly observed in patients with repaired TOF leads to progressive right ventricular dilatation and dysfunction. Therefore, imaging surveillance to monitor right ventricular volume and function using either CT or MRI is of critical importance

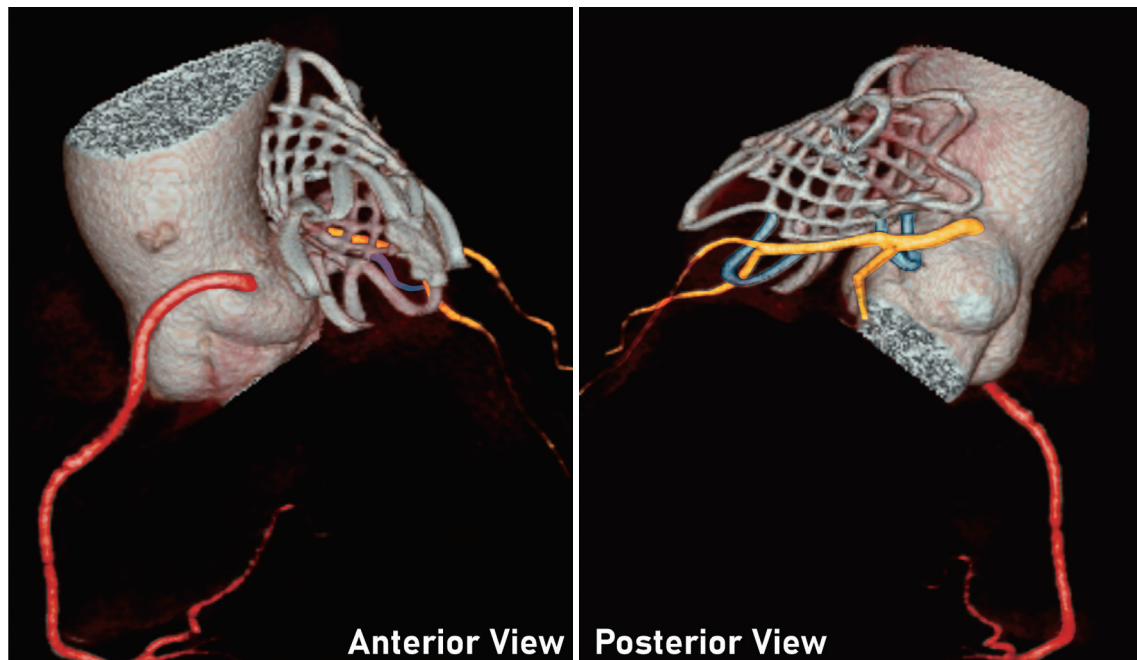


**Fig. 5.** A 21-year-old male with repaired tetralogy of Fallot who underwent percutaneous pulmonary valve implantation with a Venus p valve. Cardiac CT was performed to determine position and integrity of the implanted valve. Anterior volume-rendered cardiac CT image demonstrates the spatial relationship between the implanted valve and the ascending Ao. Posterior view reveals the LCA (yellow color) in close proximity to the valve struts (blue color), but without coronary artery compression. The RCA is coded in red color. Ao = aorta, LCA = left coronary artery, RCA = right coronary artery

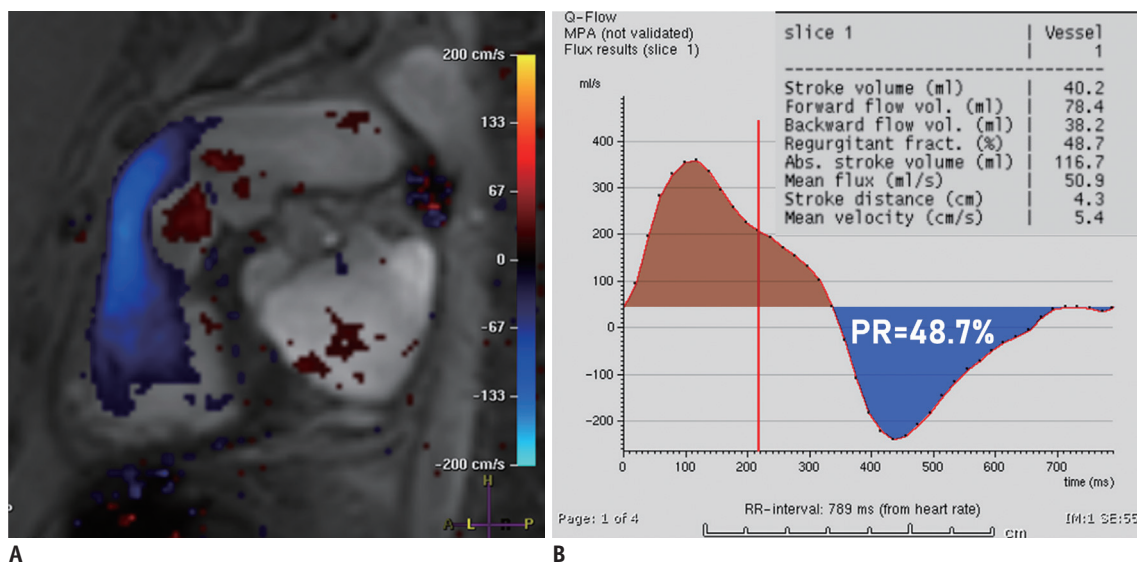


**Fig. 6.** A 27-year-old female with repaired tetralogy of Fallot using a transannular patch.

**A.** Cine MRI demonstrates a regurgitant jet (blue color) below the pulmonary valve plane. **B.** Graph of the pulmonary arterial flow volume result of phase-contrast MRI shows antegrade flow during systole (red) and retrograde flow during diastole (blue). The calculated PR fraction was 48.7%. MPA = main pulmonary artery

to determine the optimal timing of pulmonary valve replacement therapy in these patients.

CT is a useful alternative to MRI for assessing right ventricular volume and function in ACHD, including repaired

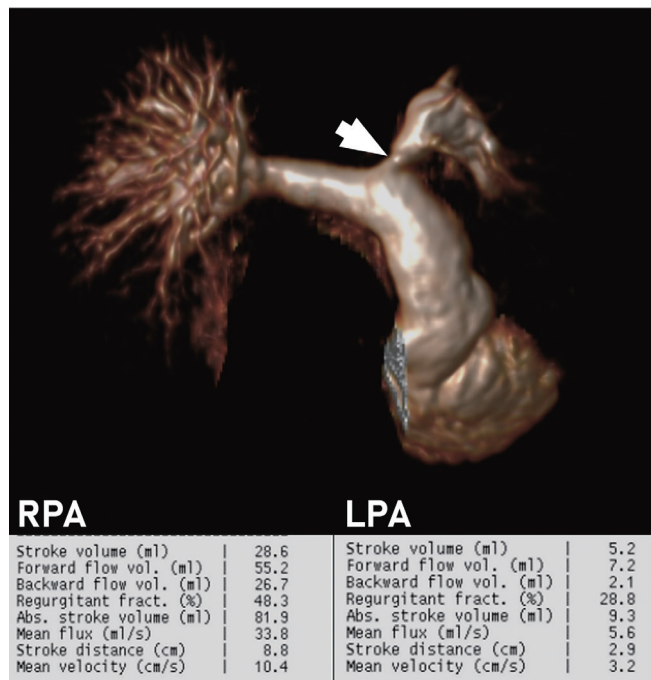


**Fig. 7. Quantitative flow analysis of the RPA and the LPA in a 10-year-old female with repaired tetralogy of Fallot.** Volume-rendered MRI with superior view shows a focal stenosis (arrow) at the proximal LPA and the diffusely dilated RPA. According to the flow quantification data, net flow through the LPA (5.2 mL) was substantially smaller than that through the RPA (28.6 mL); regurgitation fraction was higher in the RPA (48.3%) than that in the LPA (28.8%). Patient subsequently underwent angioplasty for the LPA stenosis. RPA = right pulmonary artery

TOF, when cardiac MRI is contraindicated or non-diagnostic because of artifacts (17, 18). CT results of right ventricular volume and function have been reported to be comparable to those of cardiac MRI (27). However, a recent meta-analysis confirmed that use of the same volumetry method, either simplified contouring or threshold-based, is necessary to achieve such an agreement between CT and MRI measurements of right ventricular volume and function (28). Retrospective electrocardiography-gated spiral or helical scanning or prospectively electrocardiography-triggered sequential scanning can be used for the assessment of right ventricular function. Typically, a triphasic injection protocol is used to ensure homogeneous opacification in both the right and left cardiac chambers (Fig. 8A) (5, 16-18). A semiautomatic three-dimensional threshold-based CT ventricular volumetry can measure the right ventricular volume with high accuracy and reproducibility in patients with repaired TOF (Fig. 8B) (29). A recent cross-sectional CT ventricular volumetry study demonstrated an early rapid increase (< 7 years after total surgical repair) followed by a slow increase and a plateau (up to approximately 34 years after total surgical repair) in the right ventricular volumes and right ventricular volume load parameters in 285 patients with repaired TOF (14).

Clinical practice guidelines published in 2019 described cardiac MRI criteria to select asymptomatic patients with repaired TOF who are suitable for pulmonary valve replacement. A candidate should have at least moderate pulmonary regurgitation and any of the following two factors: 1) severe right ventricular dilatation (indexed end-

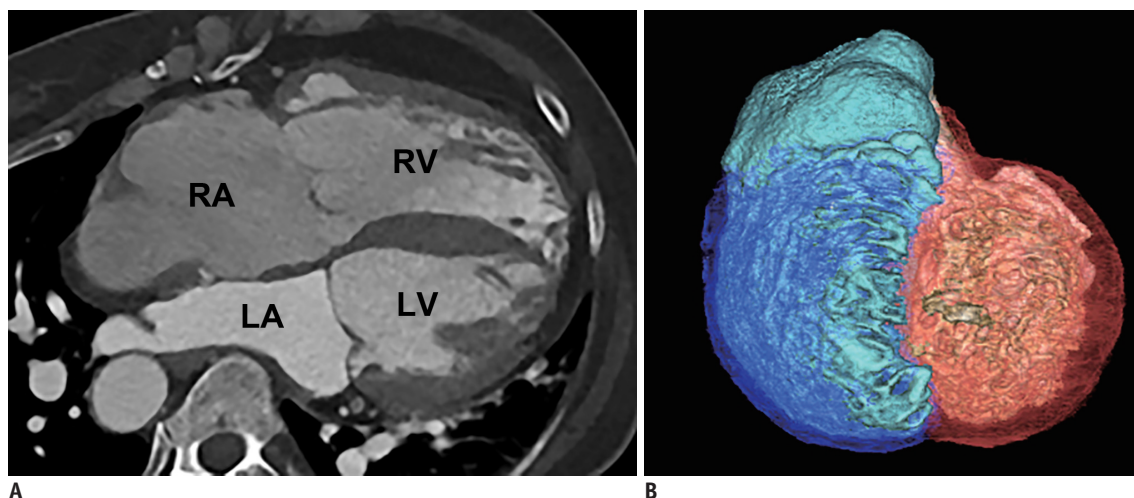


**Fig. 8. A 43-year-old female with repaired tetralogy of Fallot who underwent pulmonary valve replacement.**

**A.** Four-chamber view of cardiac CT obtained from a triphasic injection protocol demonstrates homogeneous opacification on both sides of the heart. **B.** Short-axis volume-rendered CT image shows the segmented volumes of the RV cavity (light blue), the RV mass (blue), the LV cavity (light pink), and the LV mass (dark pink) using a three-dimensional threshold-based approach. LA = left atrium

diastolic volume  $\geq 160$  mL/m<sup>2</sup>, indexed end-systolic volume  $\geq 80$  mL/m<sup>2</sup>, or right-to-left ventricular volume ratio  $\geq 2$ ; 2) mild or moderate right or left ventricular systolic dysfunction; and 3) RVOT obstruction with a peak pressure  $\geq 2/3$  of the systemic pressure (1). The ventricular volumes were typically segmented using a simplified contouring method and included papillary muscles and trabeculations. Other clinical criteria included significant cardiovascular symptoms or cardiac arrhythmias, QRS prolongation, and reduced exercise capacity (22).

### Other Complications

Left ventricular function should also be evaluated, as it is an important risk factor for adverse outcomes and is observed in  $\geq 20\%$  of patients with repaired TOF (8). The proposed mechanism of left ventricular dysfunction includes preoperative myocardial hypoxemia, myocardial fibrosis, left ventricular dyssynchrony, right ventricular dysfunction, and ventricular-ventricular interaction (30).

Although aortic root dilatation is commonly seen in patients with repaired TOF, severe dilatation ( $\geq 5$  cm) is uncommonly seen and has been reported in 8% of cases (31). Canadian guidelines suggest surgical intervention when the aortic root is greater than 5.5 cm in diameter (32). Aortic root dilatation can be measured accurately using both CT and MRI. Recently, hemodynamic abnormalities, such as flow eccentricity and increased kinetic energy, in the ascending aorta were evaluated using four-dimensional flow MRI in patients with repaired TOF (33, 34).

Late gadolinium enhancement MRI was used to identify myocardial fibrosis. Focal myocardial fibrosis at the junction between the right and left ventricular septum commonly seen in patients with repaired TOF has no clinical implications. On the other hand, myocardial fibrosis in other regions may be associated with exercise intolerance (Fig. 9) (35). In contrast, diffuse myocardial fibrosis, which can be quantified using post-contrast myocardial T1 mapping and extracellular volume mapping, is associated with adverse ventricular remodeling in patients with repaired TOF (36).

### Transposition of the Great Arteries after the Arterial Switch Operation

The arterial switch operation is the standard treatment for TGA with an intact interventricular septum, first introduced by Dr. Jatene et al. (37) in 1976. This procedure has advantages over atrial switch procedures and can avoid

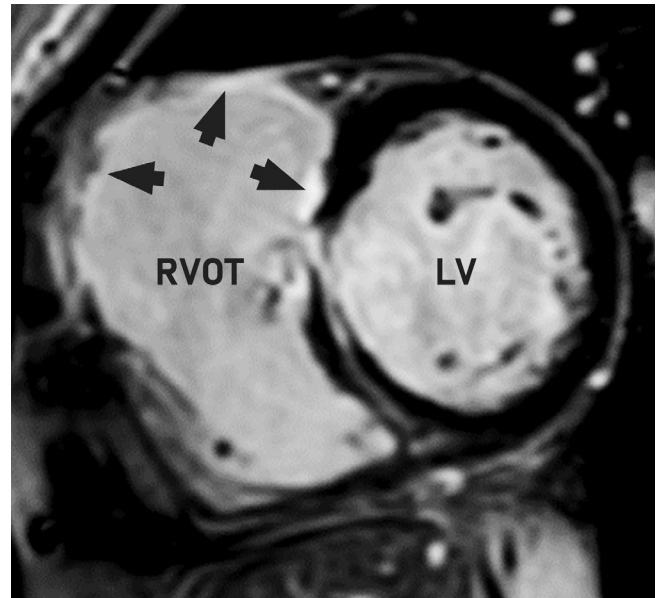


**Fig. 9.** Late gadolinium enhancement cardiac MRI in a 29-year-old female with repaired tetralogy of Fallot reveals extensive delayed enhancement (arrows) in the RVOT.

late complications of systemic right ventricular failure (37). It consists of transection of the great arteries above the valve sinuses, anastomosis of the resected great arteries to the proper ventricles using the Lecompte maneuver, and implantation of the coronary arteries into the neo-aorta. Postoperative complications include supravalvular pulmonary stenosis and neopulmonary obstruction, neo-aortic root dilatation, ventricular dysfunction, and myocardial ischemia or coronary artery stenosis, and require serial life-long imaging follow-up (Fig. 10). Since these patients are prone to sinus node dysfunction and heart block, pacing wires are frequently placed, which leads to a contraindication for MRI (17). Both CT and MRI can be used for morphological cardiovascular assessment. Coronary CT angiography is frequently used for evaluating coronary complications (38, 39), while myocardial stress perfusion MRI may be used to detect myocardial ischemia (40).

### Supravalvular Pulmonary Stenosis and Neopulmonary Artery Obstruction

Supravalvular stenosis and neopulmonary artery obstruction are the most common complications in patients following the arterial switch operation (41). However, significant obstruction requiring intervention, defined by a peak systolic gradient of  $> 50$  mm Hg, occurs only in approximately 18% of cases (42). Of interest, the frequency of left pulmonary artery stenosis requiring intervention

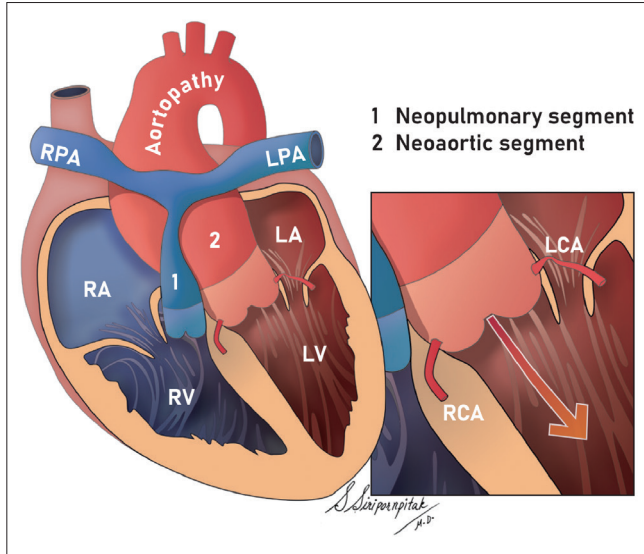


**Fig. 10. Schematic drawing illustrating complications after arterial switch operation in a patient with transposition of the great arteries, including stenosis of the neopulmonary segment, RPA, and LPA, and aortic root dilatation with aortic regurgitation (red arrow). Kinking of the LCA may be a late complication.**

is two times higher than that of the right pulmonary artery (41). The postulated mechanism for left pulmonary artery stenosis is the greater rightward position of the neopulmonary root and aortic root dilatation (Fig. 11) (43).

CT provides excellent anatomic evaluation of the pulmonary arteries following the arterial switch operation (4, 17). In particular, CT is an ideal imaging tool for assessing pulmonary artery stents (4, 17), whereas MRI may provide hemodynamic evaluation of the pulmonary blood flow. Most patients (70%) following the arterial switch operation have a balanced flow (Fig. 12) (43).

**Coronary Artery Stenosis**

The arterial switch operation requires anastomosis of the coronary arteries to the neo-aorta; therefore, the transferred coronary arteries should be evaluated carefully. The recently reported incidence of late coronary artery stenosis varies in the range of 8.9–11.3% (44, 45). The incidence seems to show a decreasing tendency chiefly due to improvements in surgical techniques used for

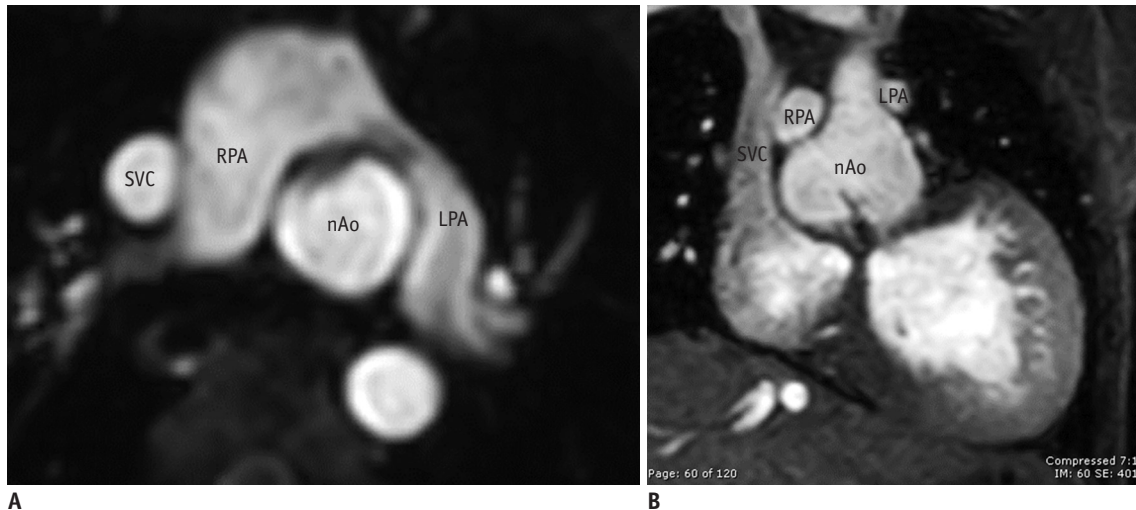


**Fig. 11. A 12-year-old female with double outlet RV who underwent arterial switch operation. Axial (A) and coronal (B) cine MRI show a narrowing of the LPA anterior to the nAo. nAo = neo-aortic segment, SVC = superior vena cava**

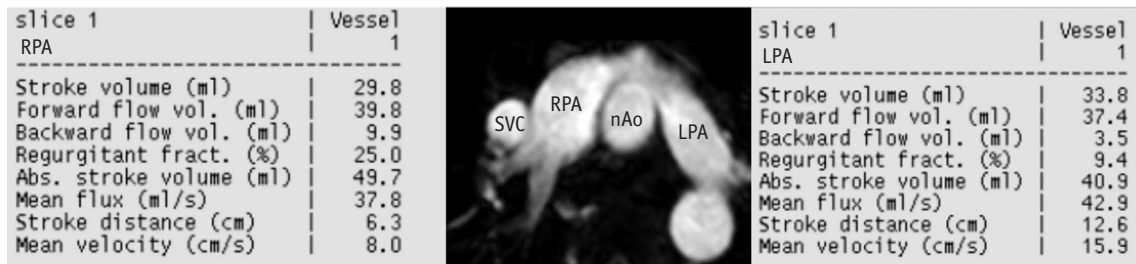


**Fig. 12. Quantitative pulmonary flow analysis using phase-contrast MRI in an 18-year-old male with transposition of the great arteries who underwent arterial switch operation. Axial cine MRI shows comparable size of the RPA and the LPA. According to the flow quantification data, branch PA flow is evenly distributed.**

coronary artery transfer. Moreover, the incidence of coronary artery abnormalities requiring changes in postoperative care, such as acute proximal angulation (Fig. 13) and high ellipticity index, diagnosed on routine coronary CT angiography in asymptomatic patients following the arterial switch operation is not trivial (24%) (39). The proximal left coronary artery is most commonly affected, and its abnormalities are caused by anterior (12–1 o'clock position) implantation on the neoaorta, resulting in an elongated course, with compression between the neoaortic and neopulmonary roots (45). CT is clearly superior to MRI for coronary artery evaluation following an arterial switch operation (4, 39, 46).

### Neoaortic Root Dilatation

A dilated neoaortic root ( $\geq$  95th percentile) is found in at least 50% of patients after an arterial switch operation (47). The neoaortic segment is rapidly dilated during the first year after the arterial switch operation, followed by an increase in size that is proportional to the somatic growth rate during childhood, and continues to increase during adulthood (48). A dilated neoaortic root not only leads to neoaortic valve regurgitation (9% increase in the hazard of aortic regurgitation  $\geq$  moderate per mm increase in aortic root diameter) (Fig. 14) but also to coronary artery compression (47-49).

CT has an established role in aortic evaluation (49), and the transferred coronary arteries can be simultaneously assessed (16, 39). On the other hand, in addition to the



**Fig. 13.** Axial cardiac CT image in a 10-year-old female who underwent arterial switch operation shows acute proximal angulation (arrow) of the RCA.

morphologic evaluation, MRI allows quantitative assessment of neo-aortic valve regurgitation (49).

### Ventricular Function and Myocardial Assessment

As previously mentioned, either CT or MRI may be used for assessing ventricular function in patients after the arterial switch operation. According to MRI findings, ventricular volume and function are typically normal in the majority of these patients, and myocardial scarring is rare (50). A recent MRI study demonstrated evidence of diffuse myocardial fibrosis in the left ventricle after the arterial switch operation, however, further studies are warranted to define its clinical significance (51).

### Functional Single Ventricle after Fontan Operation

Fontan operation is a standard surgical palliation for functional single ventricle or complex congenital heart disease in which biventricular repair is not achievable. Common functional single ventricle includes tricuspid atresia and hypoplastic left heart syndrome respectively.

The Fontan palliation initially proposed by Fontan and Baudet (52) in 1971 for the operative treatment of tricuspid atresia has undergone several revisions, including atriopulmonary connection, lateral tunnel, and extracardiac

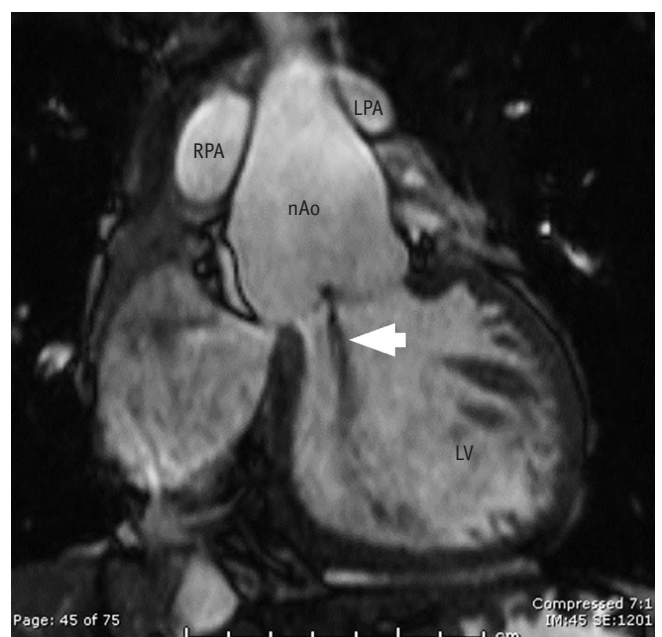


**Fig. 14.** A 15-year-old male with transposition of the great arteries who underwent arterial switch operation. Coronal cine MRI demonstrates a dilated nAo with mild aortic regurgitation (arrow) toward the LV.

conduit. The main objective of the procedure is to achieve near-normal arterial saturation and avoid volume overload on the functional single ventricle by rerouting all of the systemic venous return to the pulmonary circulation without passing through the ventricle (Fig. 15) (52). This is achieved by creating an inferior cavopulmonary connection after bidirectional superior cavopulmonary connection (Glenn shunt) in a staged manner. Fenestration in the Fontan conduit may be created to maintain preload and elude elevation of central venous pressure at the expense of mild cyanosis. The hemodynamic state following the Fontan operation may be characterized by chronic low cardiac output and non-pulsatile pulmonary arterial flow (53). Fontan-related morbidity notoriously involves multiple organ systems. Cardiothoracic complications after the Fontan

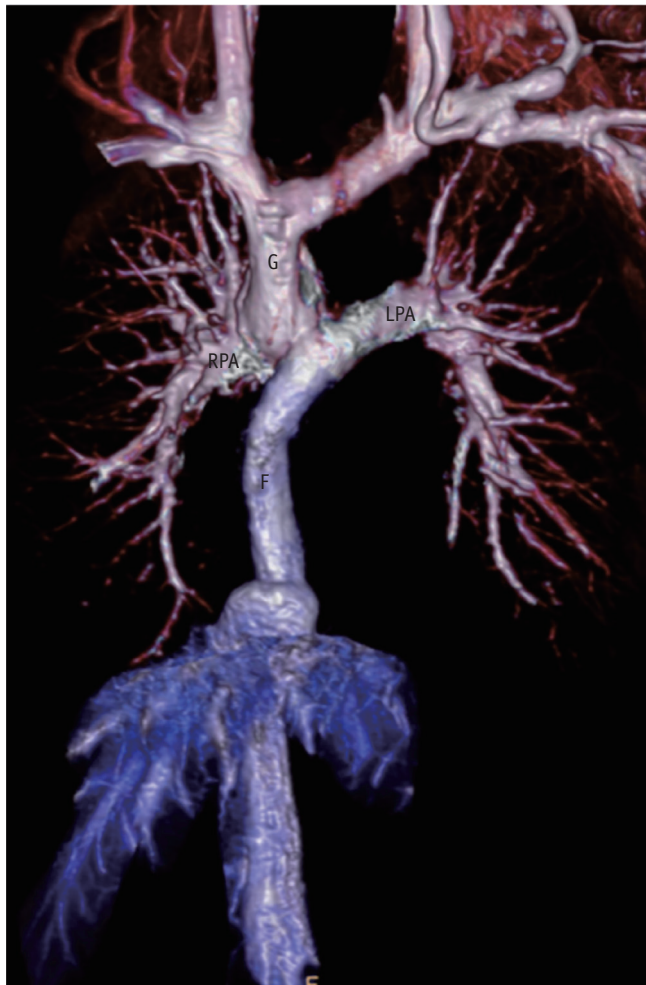


**Fig. 15.** In a 25-year-old male with functional single ventricle who underwent Fontan operation, frontal volume-rendered image of contrast-enhanced magnetic resonance angiography demonstrates the entire Fontan pathway. F = Fontan conduit, G = Glenn shunt

operation include thromboembolism, collateral vessels, cardiac dysfunction, aortopathy, pulmonary arteriovenous malformation, lymphatic abnormalities, and plastic bronchitis (Fig. 16) (54-58). CT or MRI is typically used to detect these complications. Compared to CT, MRI is used more often in clinical practice and provides comprehensive evaluation in surveillance after the Fontan operation (59). In contrast, CT is useful for identifying pulmonary thromboembolism and plastic bronchitis (55, 57).

### Patency of the Fontan Pathway

Patency of the Fontan pathway is crucial for maintaining low pulmonary vascular resistance and pulmonary arterial pressure, thereby preventing detrimental multi-organ complications. CT or MRI may be used to evaluate patency of the Fontan pathway and identify stenosis and thromboembolism (17, 60).

Sluggish, turbulent, and preferential cavopulmonary flow in the Fontan pathway requires dedicated intravenous injection of iodinated contrast agents to obtain homogeneous enhancement on CT (5, 53, 54). Various injection protocols, including simultaneous arm and leg injection, early and delayed (3 minutes) scans, recirculation phase scan (around 60 seconds), and split-bolus injection (5, 16, 17, 61, 62), have been utilized for the optimal

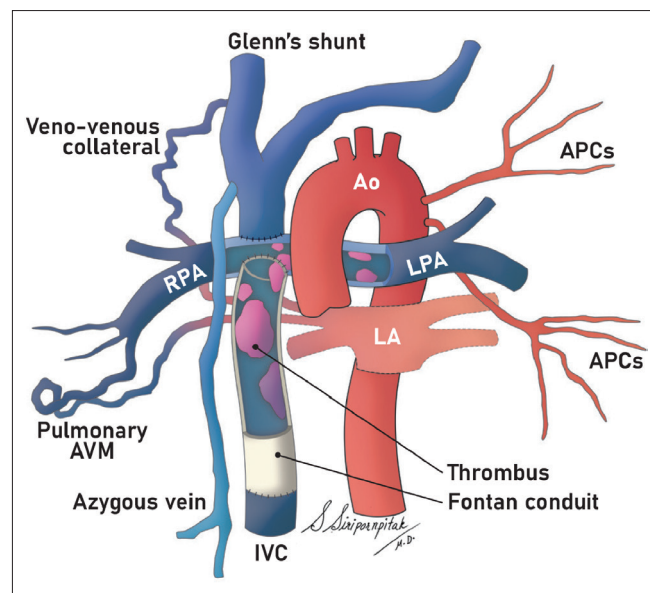


**Fig. 16.** Schematic drawing illustrating cardiopulmonary complications in patients after Fontan operation. Thrombus may occur anywhere in the entire Fontan pathway. Major forms of collateral vessels developed in the Fontan pathway are veno-venous collaterals, APCs, and AVM. APCs = aortopulmonary collaterals, AVM = arteriovenous malformation, IVC = inferior vena cava

visualization of the Fontan pathway. A recent study based on time-resolved magnetic resonance angiography in adult patients previously treated with the Fontan operation proposed 70 seconds as the optimal timing for single-phase CT angiography with an upper limb injection (63). CT obtained with an optimized contrast injection protocol is useful in detecting thromboembolism in the Fontan



**Fig. 17.** A 21-year-old female with late Fontan failure. Cardiac CT image demonstrates a thrombus (white arrow) in the Fontan conduit causing complete obstruction. In addition, the dilated azygous vein (black arrow) is noted.

pathway (Fig. 17) (55). Notably, suboptimal early CT scans often produce a false lesion in the Fontan pathway because of incomplete mixing between the iodinated contrast agent and blood (Fig. 18).

On both balanced steady-state free precession and contrast-enhanced MRI, thrombus appears as a hypointense lesion in the Fontan pathway (64, 65). Direct thrombus MRI using an inversion recovery water-selective fast gradient-echo acquisition may be used to highlight a hyperintense acute thrombus by nullifying the signals from fat (66). In addition to the morphologic evaluation of the Fontan pathway, MRI also provides comprehensive hemodynamic evaluation using time-resolved magnetic resonance angiography, conventional phase-contrast imaging, and four-dimensional flow imaging (53, 60, 63). It may be technically difficult to obtain a proper right pulmonary artery plane for phase-contrast MRI because of the close proximity of a typical bidirectional cavopulmonary connection to the proximal descending lobar branch of the right pulmonary artery. Depending on preferential cavopulmonary flow patterns, hepatic venous flow is asymmetrically distributed to the right or left lung, and the lung receiving small or no hepatic venous flow is prone to develop pulmonary arteriovenous malformation. The inferior vena caval flow distribution to the pulmonary arteries, which is crucial for predicting such risk, can be quantified



**Fig. 18.** In a 17-year-old female after Fontan operation, two-phase cardiac CT was obtained with contrast administration via a left upper arm vein.

**A.** Coronal early-phase CT image shows pseudo-thromboembolism in the PA (black arrow) and Fontan conduit (white arrow) due to preferential flow and incomplete contrast medium mixing. **B.** Coronal delayed-phase CT image confirms patent Fontan pathway (black and white arrows) without thromboembolism.

using four-dimensional flow imaging (67).

### Collateral Vessels

Collateral vessels that develop in patients after the Fontan operation include veno-venous and aortopulmonary collaterals (68, 69). In these patients, veno-venous collaterals have a negative effect on a right-to-left shunt leading to desaturation, and aortopulmonary collaterals



**Fig. 19.** In a 21-year-old female after Fontan operation, coronal cardiac CT image demonstrates several small APCs (arrows).

have a harmful effect on volume load and elevated pulmonary artery pressure. The benefits of embolization of veno-venous collaterals to improve survival in these patients are not evident and should be carefully evaluated (68). Similarly, the clinical significance of aortopulmonary collaterals as well as the indication for occluding them is not well established (69).

For better delineation of these collateral vessels on CT, we need to acquire an early phase CT (Fig. 19) (70). CT is the imaging modality of choice for evaluating residual or recurrent collateral vessels after embolization (Fig. 20). Conventional three-dimensional or time-resolved contrast-enhanced magnetic resonance angiography may be used to depict these collateral vessels in patients who underwent the Fontan procedure. However, in contrast to CT, evaluation of small-sized vessels with MRI may be limited because of the relatively low spatial resolution. Furthermore, phase-contrast MRI can provide quantification of the aortopulmonary collateral flow volume (71). However, its indication remains controversial because of inaccuracies in multiple measurements, additional acquisition time with technical difficulties for pulmonary venous flow measurement, and insufficient evidence for the beneficial effect of embolization (69). Therefore, MRI quantification of aortopulmonary collaterals is not widely used in practice.

### Ventricular Function

Accurate assessment of ventricular function is one of

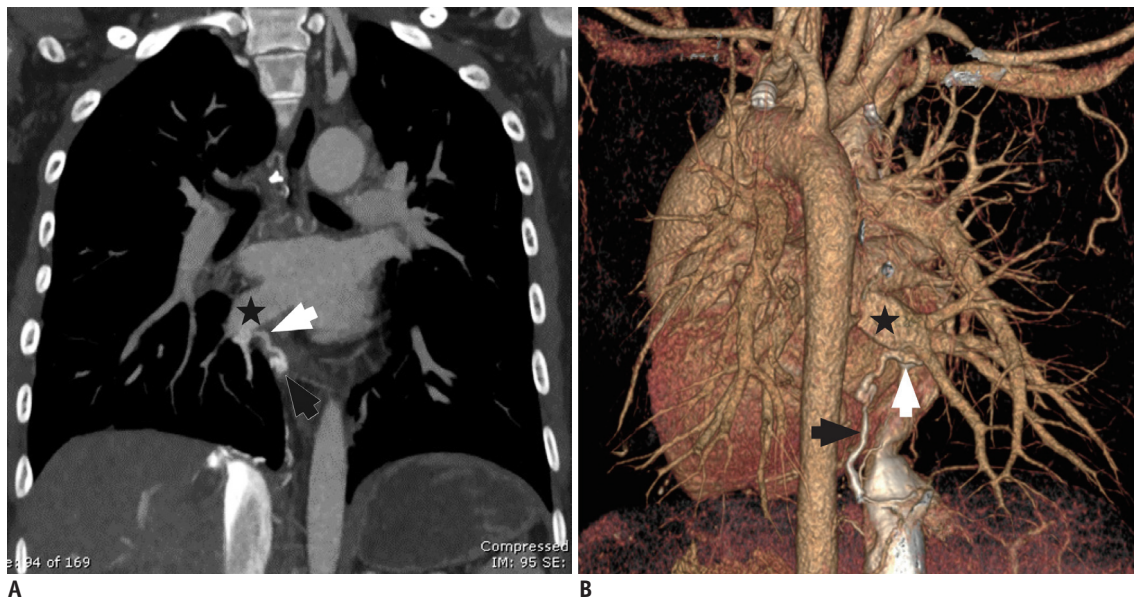


**Fig. 20.** A 16-year-old female with functional single ventricle who underwent Fontan operation. Coronal (A) and posterior volume-rendered (B) CT images reveal a veno-venous collateral (black and white arrows) between the IVC and the right inferior pulmonary vein (stars).

the essential elements in the management of patients with functional single ventricle after the Fontan operation.

As previously mentioned, CT may be used to assess ventricular function in patients with contraindications to MRI. Recently, a semiautomatic three-dimensional threshold-based CT ventricular volumetry was used to demonstrate serial changes in systemic right ventricular function early and late after the Norwood procedure in patients with hypoplastic left heart syndrome (72). In fact, a three-dimensional threshold-based segmentation approach may be more suitable than a two-dimensional simplified contouring approach for providing accurate volume of functional single ventricle with exceedingly complex

morphology and geometry. In current practice, MRI is used more often for assessing ventricular function in functional single ventricle (73). Indexed end-diastolic volume > 125 mL/m<sup>2</sup> measured using MRI is an independent predictor of a poor Fontan outcome, including transplantation or death (74). Furthermore, global strain and dyssynchrony of the single ventricle measured using feature-tracking cine MRI are independent predictors of major adverse cardiac events in these patients (75).

**Lymphatic Abnormalities and Plastic Bronchitis**

Lymphatic abnormalities in patients who have undergone the Fontan procedure are associated with severe

**Table 1. Clinical Applications of CT and MRI in Repaired Complex Adult Congenital Heart Disease**

	CT	MRI
<b>Repaired tetralogy of Fallot</b>		
Morphology of the right ventricular outflow tract and pulmonary artery		
Anatomy	++ Particularly useful for evaluating vascular stent, prosthetic valve, and calcified homograft; also for evaluating peripheral pulmonary stenosis	+
Coronary compression on the right ventricular outflow tract	++	+
Pulmonary regurgitation	+	++
Right ventricular volume and function	++ Particularly useful for patients with pacemaker or contraindicated for MRI	++
Left ventricular volume and function	++	++
Aortic root dilatation	++	++
Myocardial fibrosis assessment	-	++
<b>Transposition of the great arteries after arterial switch operation</b>		
Supravulvular pulmonary and neopulmonary segments		
Morphology	++ Particularly useful in patients with pulmonary artery stent	++
Hemodynamic assessment	-	++
Coronary artery	++	+
Neo-aortic root		
Morphology	++	++
Hemodynamic assessment	-	++
Ventricular function and volume	++	++
Myocardial fibrosis assessment	-	++
<b>Functional single ventricle after Fontan operation</b>		
Fontan pathway		
Thrombus and morphology	++	++
Hemodynamic assessment	-	++
Collateral vessels	++	+
Ventricular function	+	++
Plastic bronchitis	++	-

+ = useful, ++ = most useful, - = not useful

complications, such as protein-losing enteropathy, plastic bronchitis, and peripheral edema (76). For the evaluation of lymphatic abnormalities in these patients, MRI using either heavily T2-weighted imaging or dynamic contrast-enhanced magnetic resonance lymphangiography has been used (56, 76, 77). On the other hand, CT is useful for the evaluation of plastic bronchitis in these patients, to identify bronchial casts and monitor treatment effects (57).

## SUMMARY

CT and MRI play an increasingly important role in multimodal life-long imaging surveillance in patients with repaired complex ACHD. In this review, contemporary clinical applications of CT and MRI are described in the three most common groups of repaired complex ACHD, including repaired TOF, TGA after the arterial switch operation, and functional single ventricle after the Fontan operation. The clinical applications of CT and MRI in these ACHD groups are summarized in Table 1. With further technical developments and clinical validations, quantitative and functional assessments using CT and MRI will improve the management of this growing cohort of adult patients.

## Conflicts of Interest

The authors have no potential conflicts of interest to disclose.

## Acknowledgments

The authors would like to acknowledge Mr. Akarapol Chongwattanaoj for his creative mind and professionalism in the preparation of the illustrations.

## ORCID iDs

Suvipaporn Siripornpitak

<https://orcid.org/0000-0002-4140-6280>

Hyun Woo Goo

<https://orcid.org/0000-0001-6861-5958>

## REFERENCES

1. Stout KK, Daniels CJ, Aboulhosn JA, Bozkurt B, Broberg CS, Colman JM, et al. 2018 AHA/ACC guideline for the management of adults with congenital heart disease: executive summary: a report of the American College of Cardiology/American Heart Association Task Force on Clinical Practice Guidelines. *J Am Coll Cardiol* 2019;73:1494-1563
2. Promphan W, Wonglikhitpanya T, Katanyuwong P, Siripornpitak S. A comparative study: right ventricular assessment in post-repaired tetralogy of Fallot patients by echocardiogram with cardiac magnetic resonance imaging. *J Med Assoc Thai* 2014;97 Suppl 6:S232-S238
3. Heng EL, Babu-Narayan SV. Repaired tetralogy of Fallot. In: Saremi F, ed. *Cardiac CT and MR for adult congenital heart disease*, 1st ed. New York: Springer, 2014:199-224
4. Bonnichsen C, Ammash N. Choosing between MRI and CT imaging in the adult with congenital heart disease. *Curr Cardiol Rep* 2016;18:45
5. Ranganath P, Singh S, Abbara S, Agarwal PP, Rajiah P. Computed tomography in adult congenital heart disease. *Radiol Clin North Am* 2019;57:85-111
6. Boni L, García E, Galletti L, Pérez A, Herrera D, Ramos V, et al. Current strategies in tetralogy of Fallot repair: pulmonary valve sparing and evolution of right ventricle/left ventricle pressures ratio. *Eur J Cardiothorac Surg* 2009;35:885-889; discussion 889-890
7. Balzer D. Pulmonary valve replacement for tetralogy of Fallot. *Methodist DeBakey Cardiovasc J* 2019;15:122-132
8. Valente AM, Geva T. How to image repaired tetralogy of Fallot. *Circ Cardiovasc Imaging* 2017;10:e004270
9. Downing TE, Kim YY. Tetralogy of Fallot: general principles of management. *Cardiol Clin* 2015;33:531-541
10. Cruz C, Pinho T, Ribeiro V, Dias CC, Silva Cardoso J, Maciel MJ. Aortic dilatation after tetralogy of Fallot repair: a ghost from the past or a problem in the future? *Rev Port Cardiol* 2018;37:549-557
11. Ait Ali L, Trocchio G, Crepez R, Stuefer J, Stagnaro N, Siciliano V, et al. Left ventricular dysfunction in repaired tetralogy of Fallot: incidence and impact on atrial arrhythmias at long term-follow up. *Int J Cardiovasc Imaging* 2016;32:1441-1449
12. Cochet H, Iriart X, Allain-Nicolai A, Camaioni C, Sridi S, Nivet H, et al. Focal scar and diffuse myocardial fibrosis are independent imaging markers in repaired tetralogy of Fallot. *Eur Heart J Cardiovasc Imaging* 2019;20:990-1003
13. Geva T. Repaired tetralogy of Fallot: the roles of cardiovascular magnetic resonance in evaluating pathophysiology and for pulmonary valve replacement decision support. *J Cardiovasc Magn Reson* 2011;13:9
14. Goo HW. Changes in right ventricular volume, volume load, and function measured with cardiac computed tomography over the entire time course of tetralogy of Fallot. *Korean J Radiol* 2019;20:956-966
15. Sachdeva R, Valente AM, Armstrong AK, Cook SC, Han BK, Lopez L, et al. ACC/AHA/ASE/HRS/ISACHD/SCAI/ SCCT/SCMR/SOPE 2020 Appropriate use criteria for multimodality imaging during the follow-up care of patients with congenital heart disease: a Report of the American College of Cardiology Solution Set Oversight Committee and Appropriate Use Criteria Task Force, American Heart Association, American Society of Echocardiography, Heart Rhythm Society, International Society for Adult Congenital Heart Disease, Society for Cardiovascular

- Angiography and Interventions, Society of Cardiovascular Computed Tomography, Society for Cardiovascular Magnetic Resonance, and Society of Pediatric Echocardiography. *J Am Coll Cardiol* 2020;75:657-703
16. Hong SH, Goo HW, Maeda E, Choo KS, Tsai IC; Asian Society of Cardiovascular Imaging Congenital Heart Disease Study Group. User-friendly, vendor-specific guideline for pediatric cardiothoracic computed tomography provided by the Asian Society of Cardiovascular Imaging Congenital Heart Disease Study Group: part 1. Imaging techniques. *Korean J Radiol* 2019;20:190-204
  17. Han BK, Lesser JR. CT imaging in congenital heart disease: an approach to imaging and interpreting complex lesions after surgical intervention for tetralogy of Fallot, transposition of the great arteries, and single ventricle heart disease. *J Cardiovasc Comput Tomogr* 2013;7:338-353
  18. Ahmed S, Johnson PT, Fishman EK, Zimmerman SL. Role of multidetector CT in assessment of repaired tetralogy of Fallot. *Radiographics* 2013;33:1023-1036
  19. Tezza M, Witsenburg M, Nieman K, van de Woestijne PC, Budde RPJ. Cardiac CT to assess the risk of coronary compression in patients evaluated for percutaneous pulmonary valve implantation. *Eur J Radiol* 2019;110:88-96
  20. Goo HW, Park SH. Pulmonary vascular volume ratio measured by cardiac computed tomography in children and young adults with congenital heart disease: comparison with lung perfusion scintigraphy. *Pediatr Radiol* 2017;47:1580-1587
  21. Goo HW. Computed tomography pulmonary vascular volume ratio can be used to evaluate the effectiveness of pulmonary angioplasty in peripheral pulmonary artery stenosis. *Korean J Radiol* 2019;20:1422-1430
  22. Chung R, Taylor AM. Imaging for preintervention planning: transcatheter pulmonary valve therapy. *Circ Cardiovasc Imaging* 2014;7:182-189
  23. Schievano S, Coats L, Migliavacca F, Norman W, Frigiola A, Deanfield J, et al. Variations in right ventricular outflow tract morphology following repair of congenital heart disease: implications for percutaneous pulmonary valve implantation. *J Cardiovasc Magn Reson* 2007;9:687-695
  24. Raman SV, Cook SC, McCarthy B, Ferketich AK. Usefulness of multidetector row computed tomography to quantify right ventricular size and function in adults with either tetralogy of Fallot or transposition of the great arteries. *Am J Cardiol* 2005;95:683-686
  25. Vaujois L, Gorincour G, Alison M, Déry J, Poirier N, Lapierre C. Imaging of postoperative tetralogy of Fallot repair. *Diagn Interv Imaging* 2016;97:549-560
  26. Giannopoulos NM, Chatzis AC, Bobos DP, Kirvassilis GV, Tsoutsinos A, Sarris GE. Tetralogy of Fallot: influence of right ventricular outflow tract reconstruction on late outcome. *Int J Cardiol* 2004;97 Suppl 1:87-90
  27. Takx RA, Moscariello A, Schoepf UJ, Barraza JM Jr, Nance JW Jr, Bastarrika G, et al. Quantification of left and right ventricular function and myocardial mass: comparison of low-radiation dose 2nd generation dual-source CT and cardiac MRI. *Eur J Radiol* 2012;81:e598-e604
  28. Kim JY, Suh YJ, Han K, Kim YJ, Choi BW. Cardiac CT for measurement of right ventricular volume and function in comparison with cardiac MRI: a meta-analysis. *Korean J Radiol* 2020;21:450-461
  29. Goo HW. Semiautomatic three-dimensional threshold-based cardiac computed tomography ventricular volumetry in repaired tetralogy of Fallot: comparison with cardiac magnetic resonance imaging. *Korean J Radiol* 2019;20:102-113
  30. Yamada M, Takahashi K, Kobayashi M, Yazaki K, Takayasu H, Akimoto K, et al. Mechanisms of left ventricular dysfunction assessed by layer-specific strain analysis in patients with repaired tetralogy of Fallot. *Circ J* 2017;81:846-854
  31. Nagy CD, Alejo DE, Corretti MC, Ravekes WJ, Crosson JE, Spevak PJ, et al. Tetralogy of Fallot and aortic root dilation: a long-term outlook. *Pediatr Cardiol* 2013;34:809-816
  32. Silversides CK, Kiess M, Beauchesne L, Bradley T, Connelly M, Niwa K, et al. Canadian Cardiovascular Society 2009 Consensus Conference on the management of adults with congenital heart disease: outflow tract obstruction, coarctation of the aorta, tetralogy of Fallot, Ebstein anomaly and Marfan's syndrome. *Can J Cardiol* 2010;26:e80-e97
  33. Lee S, Kim YJ, Jung JW, Choi JY, Park HK, Shin YR, et al. Evaluation of flow pattern in the ascending aorta in patients with repaired tetralogy of Fallot using four-dimensional flow magnetic resonance imaging. *Korean J Radiol* 2019;20:1334-1341
  34. Robinson JD, Rose MJ, Joh M, Jarvis K, Schnell S, Barker AJ, et al. 4-D flow magnetic-resonance-imaging-derived energetic biomarkers are abnormal in children with repaired tetralogy of Fallot and associated with disease severity. *Pediatr Radiol* 2019;49:308-317
  35. Wald RM, Haber I, Wald R, Valente AM, Powell AJ, Geva T. Effects of regional dysfunction and late gadolinium enhancement on global right ventricular function and exercise capacity in patients with repaired tetralogy of Fallot. *Circulation* 2009;119:1370-1377
  36. Kozak MF, Redington A, Yoo SJ, Seed M, Greiser A, Grosse-Wortmann L. Diffuse myocardial fibrosis following tetralogy of Fallot repair: a T1 mapping cardiac magnetic resonance study. *Pediatr Radiol* 2014;44:403-409
  37. Jatene AD, Fontes VF, Paulista PP, Souza LC, Neger F, Galantier M, et al. Anatomic correction of transposition of the great vessels. *J Thorac Cardiovasc Surg* 1976;72:364-370
  38. Goo HW, Seo DM, Yun TJ, Park JJ, Park IS, Ko JK, et al. Coronary artery anomalies and clinically important anatomy in patients with congenital heart disease: multislice CT findings. *Pediatr Radiol* 2009;39:265-273
  39. Szymczyk K, Moll M, Sobczak-Budlewska K, Moll JA, Stefańczyk L, Grzelak P, et al. Usefulness of routine coronary CT angiography in patients with transposition of the great arteries after an arterial switch operation. *Pediatr Cardiol* 2018;39:335-346

40. Noel CV, Krishnamurthy R, Masand P, Moffett B, Schlingmann T, Cheong BY, et al. Myocardial stress perfusion MRI: experience in pediatric and young-adult patients following arterial switch operation utilizing regadenoson. *Pediatr Cardiol* 2018;39:1249-1257
41. Serraf A, Roux D, Lacour-Gayet F, Touchot A, Bruniaux J, Sousa-Uva M, et al. Reoperation after the arterial switch operation for transposition of the great arteries. *J Thorac Cardiovasc Surg* 1995;110:892-899
42. Delmo Walter EM, Miera O, Nasser B, Huebler M, Alexi-Meskishvili V, Berger F, et al. Onset of pulmonary stenosis after arterial switch operation for transposition of great arteries with intact ventricular septum. *HSR Proc Intensive Care Cardiovasc Anesth* 2011;3:177-187
43. Morgan CT, Mertens L, Grotenhuis H, Yoo SJ, Seed M, Grosse-Wortmann L. Understanding the mechanism for branch pulmonary artery stenosis after the arterial switch operation for transposition of the great arteries. *Eur Heart J Cardiovasc Imaging* 2017;18:180-185
44. Tsuda T, Bhat AM, Robinson BW, Baffa JM, Radtke W. Coronary artery problems late after arterial switch operation for transposition of the great arteries. *Circ J* 2015;79:2372-2379
45. Ou P, Khraiche D, Celermajer DS, Agnoletti G, Le Quan Sang KH, Thalabard JC, et al. Mechanisms of coronary complications after the arterial switch for transposition of the great arteries. *J Thorac Cardiovasc Surg* 2013;145:1263-1269
46. Cohen MS, Eidem BW, Cetta F, Fogel MA, Frommelt PC, Ganame J, et al. Multimodality imaging guidelines of patients with transposition of the great arteries: a report from the American Society of Echocardiography developed in collaboration with the Society for Cardiovascular Magnetic Resonance and the Society of Cardiovascular Computed Tomography. *J Am Soc Echocardiogr* 2016;29:571-621
47. Schwartz ML, Gauvreau K, del Nido P, Mayer JE, Colan SD. Long-term predictors of aortic root dilation and aortic regurgitation after arterial switch operation. *Circulation* 2004;110:128-132
48. van der Palen RLF, van der Bom T, Dekker A, Tsonaka R, van Geloven N, Kuipers IM, et al. Progression of aortic root dilatation and aortic valve regurgitation after the arterial switch operation. *Heart* 2019;105:1732-1740
49. Michalak KW, Sobczak-Budlewska K, Moll JJ, Szymczyk K, Moll JA, Łubisz M, et al. Neo-aortic regurgitation in patients with transposition long term after an arterial switch operation and its relation to the root diameters and surgical technique used. *Pediatr Cardiol* 2020;41:31-37
50. Shepard CW, Germanakis I, White MT, Powell AJ, Co-Vu J, Geva T. Cardiovascular magnetic resonance findings late after the arterial switch operation. *Circ Cardiovasc Imaging* 2016;9:e004618
51. Grotenhuis HB, Cifra B, Mertens LL, Riessenkampff E, Manlhiot C, Seed M, et al. Left ventricular remodelling in long-term survivors after the arterial switch operation for transposition of the great arteries. *Eur Heart J Cardiovasc Imaging* 2019;20:101-107
52. Fontan F, Baudet E. Surgical repair of tricuspid atresia. *Thorax* 1971;26:240-248
53. Whitehead KK, Sundaeswaran KS, Parks WJ, Harris MA, Yoganathan AP, Fogel MA. Blood flow distribution in a large series of patients having the Fontan operation: a cardiac magnetic resonance velocity mapping study. *J Thorac Cardiovasc Surg* 2009;138:96-102
54. Ohuchi H. Adult patients with Fontan circulation: what we know and how to manage adults with Fontan circulation? *J Cardiol* 2016;68:181-189
55. Ghadimi Mahani M, Agarwal PP, Rigsby CK, Lu JC, Fazeli Dehkordy S, Wright RA, et al. CT for assessment of thrombosis and pulmonary embolism in multiple stages of single-ventricle palliation: challenges and suggested protocols. *Radiographics* 2016;36:1273-1284
56. Biko DM, DeWitt AG, Pinto EM, Morrison RE, Johnstone JA, Griffis H, et al. MRI evaluation of lymphatic abnormalities in the neck and thorax after Fontan surgery: relationship with outcome. *Radiology* 2019;291:774-780
57. Goo HW, Jhang WK, Kim YH, Ko JK, Park IS, Park JJ, et al. CT findings of plastic bronchitis in children after a Fontan operation. *Pediatr Radiol* 2008;38:989-993
58. Caruthers RL, Kempa M, Loo A, Gulbransen E, Kelly E, Erickson SR, et al. Demographic characteristics and estimated prevalence of Fontan-associated plastic bronchitis. *Pediatr Cardiol* 2013;34:256-261
59. Zaki NC, Kelleman MS, James Parks W, Slesnick TC, McConnell ME, Oster ME. The utility of cardiac magnetic resonance imaging in post-Fontan surveillance. *Congenit Heart Dis* 2019;14:140-146
60. Goo HW, Yang DH, Park IS, Ko JK, Kim YH, Seo DM, et al. Time-resolved three-dimensional contrast-enhanced magnetic resonance angiography in patients who have undergone a Fontan operation or bidirectional cavopulmonary connection: initial experience. *J Magn Reson Imaging* 2007;25:727-736
61. Greenberg SB, Bhutta ST. A dual contrast injection technique for multidetector computed tomography angiography of Fontan procedures. *Int J Cardiovasc Imaging* 2008;24:345-348
62. Park EA, Lee W, Chung SY, Yin YH, Chung JW, Park JH. Optimal scan timing and intravenous route for contrast-enhanced computed tomography in patients after Fontan operation. *J Comput Assist Tomogr* 2010;34:75-81
63. Duerden L, Abdullah H, Lyen S, Manghat N, Hamilton M. Contrast circulation in adult fontan patients using MR time resolved angiography: application for CT pulmonary angiography. *J Cardiovasc Comput Tomogr* 2020;14:330-334
64. Casolo G, Rega L, Gensini GF. Detection of right atrial and pulmonary artery thrombosis after the Fontan procedure by magnetic resonance imaging. *Heart* 2004;90:825
65. Caro-Dominguez P, Yoo SJ, Seed M, Grosse-Wortmann L. Magnetic resonance imaging of cardiovascular thrombi in children. *Pediatr Radiol* 2018;48:722-731
66. Mendichovszky IA, Priest AN, Bowden DJ, Hunter S, Joubert

- I, Hilborne S, et al. Combined MR direct thrombus imaging and non-contrast magnetic resonance venography reveal the evolution of deep vein thrombosis: a feasibility study. *Eur Radiol* 2017;27:2326-2332
67. Sundareswaran KS, Haggerty CM, de Zélicourt D, Dasi LP, Pekkan K, Frakes DH, et al. Visualization of flow structures in Fontan patients using 3-dimensional phase contrast magnetic resonance imaging. *J Thorac Cardiovasc Surg* 2012;143:1108-1116
68. Poterucha JT, Johnson JN, Taggart NW, Cabalka AK, Hagler DJ, Driscoll DJ, et al. Embolization of veno-venous collaterals after the Fontan operation is associated with decreased survival. *Congenit Heart Dis* 2015;10:E230-E236
69. Powell AJ. Aortopulmonary collaterals in single-ventricle congenital heart disease: how much do they count? *Circ Cardiovasc Imaging* 2009;2:171-173
70. Goo HW. Haemodynamic findings on cardiac CT in children with congenital heart disease. *Pediatr Radiol* 2011;41:250-261
71. Grosse-Wortmann L, Al-Otay A, Yoo SJ. Aortopulmonary collaterals after bidirectional cavopulmonary connection or Fontan completion: quantification with MRI. *Circ Cardiovasc Imaging* 2009;2:219-225
72. Goo HW. Serial changes in anatomy and ventricular function on dual-source cardiac computed tomography after the Norwood procedure for hypoplastic left heart syndrome. *Pediatr Radiol* 2017;47:1776-1786
73. Margossian R, Schwartz ML, Prakash A, Wruck L, Colan SD, Atz AM, et al. Comparison of echocardiographic and cardiac magnetic resonance imaging measurements of functional single ventricular volumes, mass, and ejection fraction (from the Pediatric Heart Network Fontan Cross-Sectional Study). *Am J Cardiol* 2009;104:419-428
74. Rathod RH, Prakash A, Kim YY, Germanakis IE, Powell AJ, Gauvreau K, et al. Cardiac magnetic resonance parameters predict transplantation-free survival in patients with fontan circulation. *Circ Cardiovasc Imaging* 2014;7:502-509
75. Ishizaki U, Nagao M, Shiina Y, Inai K, Mori H, Takahashi T, et al. Global strain and dyssynchrony of the single ventricle predict adverse cardiac events after the Fontan procedure: analysis using feature-tracking cine magnetic resonance imaging. *J Cardiol* 2019;73:163-170
76. Mohanakumar S, Telinius N, Kelly B, Lauridsen H, Boedtkjer D, Pedersen M, et al. Morphology and function of the lymphatic vasculature in patients with a Fontan circulation. *Circ Cardiovasc Imaging* 2019;12:e008074
77. Zheng Q, Itkin M, Fan Y. Quantification of thoracic lymphatic flow patterns using dynamic contrast-enhanced MR lymphangiography. *Radiology* 2020;296:202-207